Journal of Nanobiotechnology

RESEARCH

Open Access

A multifunctional PEGylated liposomal-encapsulated sunitinib enhancing autophagy, immunomodulation, and safety in renal cell carcinoma

Po-Fu Yueh[1], Chih-Sheng Chiang[2,3], I-Jung Tsai[3], Yun-Long Tseng[4], He-Ru Chen[4], Keng-Li Lan[1,5,7*†] and Fei-Ting Hsu[6*†]

Abstract

Background Sunitinib is a multikinase inhibitor used to treat patients with advanced renal cell carcinoma (RCC). However, sunitinib toxicity makes it a double-edged sword. Potent immune modulation by sunitinib extends to nuclear interactions. To address these issues, there is an urgent need for delivery vectors suitable for sunitinib treatment.

Methods We developed PEGylated liposomes as delivery vectors to precisely target sunitinib (lipo-sunitinib) to RCC tumors. Further investigations, including RNA sequencing (RNA-seq), were performed to evaluate transcriptomic changes in these pathways. DiI/DiR-labeled lipo-sunitinib was used for the biodistribution analysis. Flow cytometry and immunofluorescence (IF) were used to examine immune modulation in orthotopic RCC models.

Results The evaluation of results indicated that lipo-sunitinib precisely targeted the tumor site to induce autophagy and was readily taken up by RCC tumor cells. In addition, transcriptomic assays revealed that following lipo-sunitinib treatment, autophagy, antigen presentation, cytokine, and chemokine production pathways were upregulated, whereas the epithelial-mesenchymal transition (EMT) pathway was downregulated. In vivo data provided evidence supporting the inhibitory effect of lipo-sunitinib on RCC tumor progression and metastasis. Flow cytometry further demonstrated that liposunitinib increased the infiltration of effector T cells (Teffs) and conventional type 1 dendritic cells (cDC1s) into the tumor. Furthermore, systemic immune organs such as the tumor-draining lymph nodes, spleen, and bone marrow exhibited upregulated anticancer immunity following lipo-sunitinib treatment.

Conclusion Our findings demonstrated that lipo-sunitinib is distributed at the RCC tumor site, concurrently inducing potent autophagy, elevating antigen presentation, activating cytokine and chemokine production pathways, and downregulating EMT in RCC cells. This comprehensive approach significantly enhanced tumor inhibition and promoted anticancer immune modulation.

Keywords Liposome, Sunitinib, Renal cell carcinoma, Drug delivery, Immune modulation

†Keng-Li Lan and Fei-Ting Hsu contributed equally.

*Correspondence:
Keng-Li Lan
kllan@vghtpe.gov.tw
Fei-Ting Hsu
sakiro920@mail.cmu.edu.tw
Full list of author information is available at the end of the article

Introduction

Renal cell carcinoma (RCC) is a formidable global health challenge and one of the most lethal malignant tumors [1]. Current standard treatments encompass surgical interventions, radiation therapy, and chemotherapy [2, 3]. In 2016, the US Food and Drug Administration (FDA) granted approval to SUTENT® (sunitinib) for the treatment of advanced RCC [4]. Clinical trial outcomes revealed that sunitinib surpasses IFN-α in both objective response rate and survival rate, establishing its efficacy as a potent multiple tyrosine kinase inhibitor (TKi) against advanced RCC [4, 5]. Sunitinib targets key tyrosine kinases, including vascular endothelial growth factor receptor 2 (VEGFR2), platelet-derived growth factor receptor-β (PDGFR-β), and KIT, impeding their activations and thereby suppressing tumor growth [6].

Recent studies have uncovered an additional dimension to the effect of sunitinib, demonstrating its ability to induce tumor immune surveillance by upregulating autophagy in cancer cells, leading to the inhibition of tumor programmed death ligand 1 (PD-L1) expression [7]. This suggests a potential influence on the tumor microenvironment (TME). Combining sunitinib with immune checkpoint inhibitors (ICIs) has shown the potential for enhancing antitumor effects, although the underlying mechanism remains unclear. However, sunitinib has significant effects on various organs of the human body. This is a double-edged sword in the treatment of patients with advanced RCC. It is associated with certain side effects and the potential for cardiotoxicity, resulting in severe and sometimes fatal side effects [8, 9]. In response to this challenge, our group designed a novel solution: a simple formulation and an innovative nanocarrier using PEGylated liposomes to encapsulate sunitinib, termed lipo-sunitinib.

PEGylated liposomes exhibit the ability to passively target tumor tissues through the enhanced permeability and retention (EPR) effect facilitated by nanoparticle extravasation and increased permeability of the tumor vasculature [10–12]. Furthermore, PEGylation of the liposome surface extends its half-life in the body by increasing the particle size [13–15]. This biocompatible material ensures a high level of patient safety. Theoretically, PEGylated liposomal encapsulation of a drug allows for a lower dosage to achieve higher efficacy, capitalizing on its unique features.

Through precise targeting of tumor cells via the EPR effect and PEGylation of lipo-sunitinib, our research successfully demonstrated augmented inhibition of RCC orthotopic tumors in mouse models. This innovative approach holds promise for mitigating the toxicity associated with sunitinib, while enhancing its therapeutic effectiveness in the treatment of advanced RCC.

Materials and methods

Characterization

The structure, size, and zeta potential of lipo-sunitinib were assessed using transmission electron microscopy (TEM, JEM-2100F, JEOL Ltd., Japan) and dynamic light scattering (DLS, Litesizer DLS 500, Anton Paar GmbH, Republic of Austria). For TEM sample preparation, lipo-sunitinib was centrifuged (8000×*g*, 10 min) and resuspended in deionized water (DDW). The TEM grid was immersed in DDW containing lipo-sunitinib for 30 s, followed by negative staining with uranyl acetate. The samples were then vacuum dried for TEM observation. To determine particle size, distribution, and zeta potential, lipo-sunitinib was suspended in phosphate-buffered saline (PBS) and subjected to DLS analysis at room temperature (20–25 °C).

Preparation of lipo-sunitinib

A gradient of ammonium sulfate (AS) to load sunitinib into the liposomes. First, the liposome vector (that is, without sunitinib) containing AS (300 mM), phospholipid (60 mM), and hydrogenated soybean phosphatidylcholine (HSPC): cholesterol at 3 of 2 was suspended in 0.9% NaCl solution. The liposome solution (10 mL) along with sunitinib (6.7 mL; 30 mg mL-1 in 0.9% NaCl), L-histidine (1 mL; 31 mg mL-1 in 0.9% NaCl) and 0.9% NaCl (2.3 mL) were added to a 50-mL tube and subjected to a vigorous shake in a 60 °C water bath. To improve homogeneity, the solution was incubated at 60 °C for 30 min every 10 min throughout the shaking process. Liposomal sunitinib was purified using a Sephadex G-50 fine gel and stored in 0.9% NaCl at 4 °C [16].

Measuring sunitinib levels using HPLC

Sunitinib levels were measured using high-performance liquid chromatography (HPLC; Vanquish Core HPLC, Thermo Fisher Scientific, USA). The analysis was performed using a Waters XTERRA® RP18 column (150 mm×4.6 mm, 3.5 μm). The mobile phase consisted of methanol: deionized water (DDW) and 0.01% trifluoroacetic acid at a ratio of 67:33. The flow rate was set at 1 mL/min, and the absorbance was measured at a wavelength of 423 nm. The column oven was maintained at 35 °C to detect the released sunitinib. The cumulative percentage of sunitinib released was calculated and plotted against time to generate the release profile.

Drug release

The in vitro drug release profile of sunitinib from lipo-sunitinib at different pH values was analyzed as follows:

Lipo-sunitinib (9.7 mg/mL, 1 mL) was loaded into a dialysis bag with a molecular weight cutoff (MWCO) of 100 kDa. The dialysis bag was placed in a beaker containing 100 mL of PBS. The system was maintained under magnetic stirring at 250 rpm and maintained at a constant temperature of 37 °C.

At specific time intervals (0.5, 1, 2, 3, 6, 12, 24, 48, 72, and 96 h), 1 mL of the release medium was withdrawn. The withdrawn samples were extracted with a solvent consisting of 50% acetonitrile. After extraction, the sample was centrifuged at 10,000×*g* and the resulting suspension was collected for analysis by high-performance liquid chromatography (HPLC, Vanquish Core HPLC, Thermo Fisher Scientific, USA). HPLC analysis was performed using a Waters XTERRA® RP18 column (150 mm × 4.6 mm, 3.5 μm). The mobile phase consisted of methanol: deionized water (DDW) and 0.01% trifluoroacetic acid at a ratio of 67:33. The flow rate was set at 1 mL/min, and the absorbance was measured at a wavelength of 423 nm. The column oven was maintained at 35 °C to detect the released sunitinib. The cumulative percentage of sunitinib released was calculated and plotted against time to generate the release profile.

Hemolysis assay

To assess the stability and safety of lipo-sunitinib in blood, we added 500 μL of PBS, water, and various concentrations of lipo-sunitinib to 50 μL of mouse whole blood. The mixture was then incubated at 37 °C for 1 h. Following incubation, blood was centrifuged at 1,000×*g* for 10 min. The resulting supernatants were transferred to a 96-well plate and analyzed by measuring the absorbance at 414 nm using SpectraMax iD3 (Molecular Devices, CA, USA) [17].

RNA sequencing (RNA-seq) & GSEA

RENCA cells were subjected to a 24-h treatment regimen with 10 μg/mL of sunitinib and 10 μg/mL of lipo-sunitinib. For RNA extraction, all cell samples were processed using an Invitrogen PureLink RNA Mini Kit (12-183-018A). The cells were initially lysed with 1% 2-mercaptoethanol in lysis buffer to ensure efficient disruption of cellular membranes and preservation of RNA integrity. Following lysis, the RNA was purified according to the manufacturer's instructions provided with the kit. The purified RNA samples were shipped to Genomics Ltd. (Taipei, Taiwan) for further processing. RNA-seq was performed using a NovaSeq 6000 platform to generate a comprehensive transcriptome profile.

The resulting RNA expression data were used for gene set enrichment analysis (GSEA) to comprehensively investigate the transcriptomic effects of lipo-sunitinib treatment. GSEA allows the identification of coordinated changes in gene expression within predefined sets of genes, providing valuable insights into biological pathways and processes affected by treatment.

Cell culture

RENCA cells and A498 cells were purchased from Bioresource Collection and Research Center (BCRC, Hsinchu City, Taiwan) and maintained in Roswell Park Memorial Institute (RPMI) 1640 and Eagle's Minimum Essential (MEM) medium contenting 10% fetal bovine serum (FBS) and 1 × penicillin/streptomycin (PS), then incubated with 5% CO_2 and 95% air mixture at 37 ℃ humanity incubator.

MTT

RENCA and A498 cells were seeded at a density of 5000 cells/well in 96-well plates and incubated at 37 °C overnight for stabilization. Next, the cells were treated with various concentrations of sunitinib and lipo-sunitinib for a 24-h treatment period. Following the treatments, the culture media was replaced with a 0.5 mg/mL MTT solution and incubated at 37 °C for an additional 1 h. To dissolve the formazan crystals, DMSO was continuously added to the cells, and the absorbance was measured at 570 nm using a SpectraMax iD3 spectrophotometer for analysis [18].

Lentivirus transduction

To generate luciferase-expressing RENCA cells, a commercial lentivirus (AS3w-FLuc-Ppuro; Academia Sinica, Taipei, Taiwan) was used to deliver the luciferase plasmid into the cells. First, we seeded fifty thousand cells per well in 24-well plates and incubated overnight. The following day, we added lentivirus to the wells at a concentration of 8 μg/mL polybrene and allowed the cells to co-culture with the virus. Transduced cells were selected using 1 μg/mL puromycin (InvivoGen, San Diego, CA, USA). To establish a stable, single clone expressing luciferase, we used a 96-well plate to screen for the clone with the highest luminescence signal, as detected using the IVIS Lumina LT Series III (PerkinElmer, Waltham, MA, USA). This clone was named RENCA/luc and used for subsequent experiments.

Animal studies

Six-week-old BALB/c mice were obtained from the National Laboratory Animal Center in Taipei, Taiwan and used to establish subcutaneous and orthotopic RCC

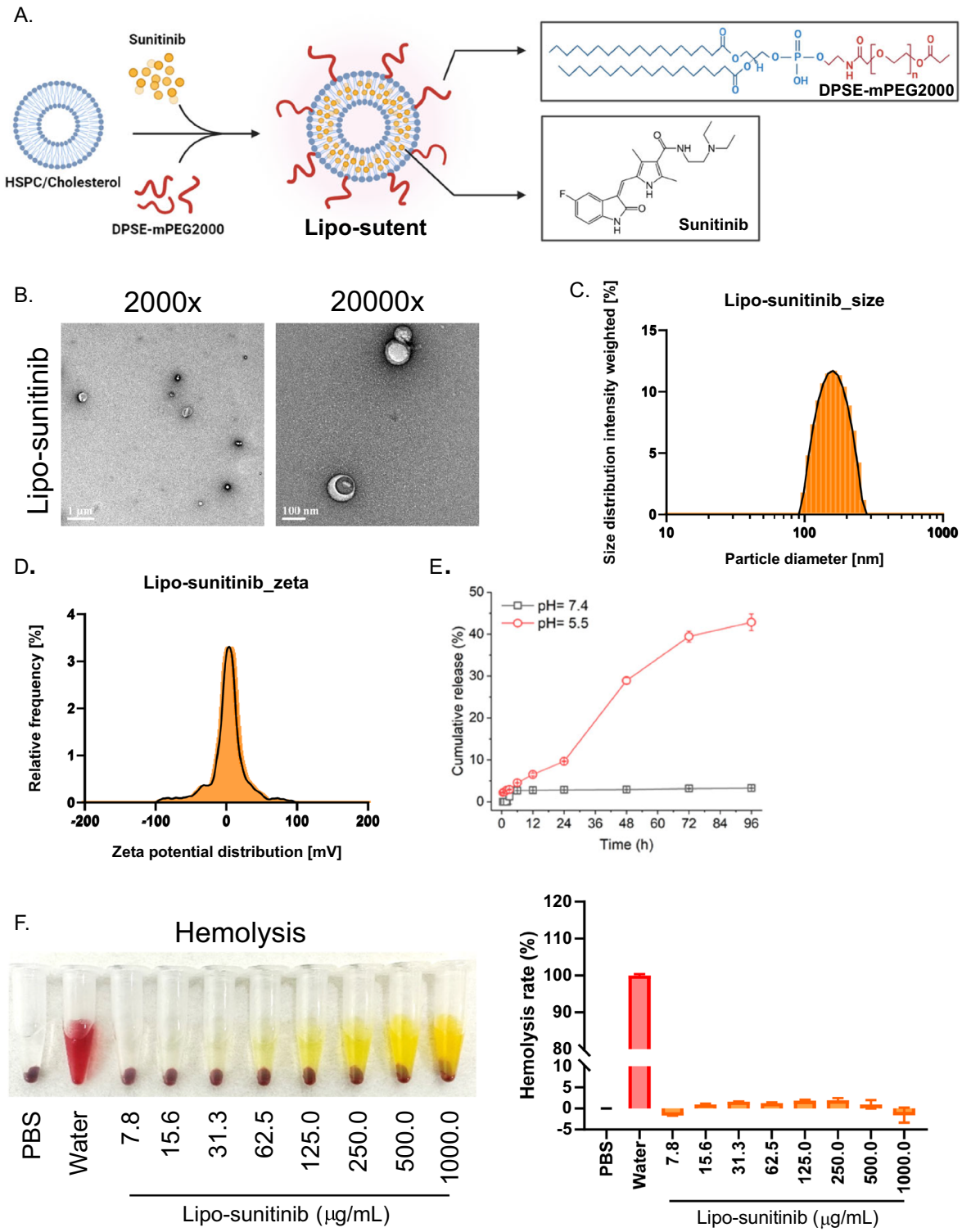

Fig. 1 The characterization of lipo-sunitinib. **A** Sunitinib was encapsulated within liposomes, and the surface was modified through PEGylation. **B** The morphology of lipo-sunitinib was examined using TEM at magnifications of ×2,000 and ×20,000. **C** The size and **D** zeta potential of lipo-sunitinib were determined using DLS. **E** A release assay was conducted to assess the liberation of sunitinib from lipo-sunitinib under lower pH (5.5) conditions. **F** A hemolysis assay was performed to evaluate the toxicity of lipo-sunitinib in the circulatory system

models. For the subcutaneous model, we inoculated five hundred thousand RENCA cells into the right leg of each mouse. Once the tumors reached a size of 100 mm^3, the subcutaneous RCC models were randomly divided into three groups: vehicle (0.1% DMSO), sunitinib (30 mg/kg), and lipo-sunitinib (10 mg/kg). The tumor volume and body weight of the mice every 2 d after treatment initiation. On day 14, the tumors were harvested for further testing.

For the orthotopic RCC model, we inoculated twenty thousand RENCA/luc cells were inoculated into the left kidney of each mouse. We tracked the orthotopic models weekly using an IVIS Lumina LT Series III. After tumor formation, the orthotopic RCC models were randomly divided into four groups: vehicle (0.1% DMSO), oral sunitinib (10 mg/kg, oral-sut), IV sunitinib (10 mg/kg, IV-sut), and lipo-sunitinib (10 mg/kg). The therapeutic efficacy of the treatment was evaluated by assessing RCC luminescence signal levels.

DiI/DiR biodistribution

To effectively monitor the in vivo biodistribution of lipo-sunitinib, we employed DiI and DiR, lipophilic dyes, to label lipo-sunitinib for a duration of 10 min, achieving a final concentration of 320 μg/mL in PBS. Next, lipo-sunitinib was washed twice with PBS and was to a concentration of 0.2 mg in 100 μL PBS. The resulting DiR-lipo-sunitinib was intravenously injected into RCC orthotopic mice, and DiR signals were tracked at 0, 4, 24, and 48 h using time-lapse imaging. Excitation and emission wavelengths were set at 710 and 760 nm, respectively, using IVIS Lumina LT Series III for imaging purposes [19].

H&E staining

We evaluated the potential toxicity of the drug using Hematoxylin and Eosin (H&E) staining of organs obtained from subcutaneous RCC models. The heart, liver, and kidneys were fixed in 10% neutral formalin (Leica, Wetzlar, Germany) and embedded in paraffin for sectioning. Tissue sections were stained with hematoxylin, de-stained with 0.5% acetic ethanol, and stained with 0.1% sodium bicarbonate before staining with eosin. We dehydrated the slides with xylene and mounted them for observation using the EVOS M5000 microscope (Invitrogen, Carlsbad, CA, USA). Our analysis of the tissue sections allowed us to assess the potential toxic effects of the drug on the examined organs.

Immunofluorescence (IF)

The tumor tissues were embedded with OCT (cryosection compound) and created the 5-μm thickness section for further staining steps. The slides were fixed with 4% paraformaldehyde and blocked with 3% bovine serum albumin (BSA) solution. The primary antibodies were diluted (1:200–1:300) with 1% BSA dilution buffer and incubated with the fixed slides. After primary antibodies incubation, the slides were treated with different fluorescence-conjugated secondary antibodies and stained with 1 μg/mL DAPI for nuclei location. Images were captured using an EVOS M5000 microscope.

Flow cytometry

Cells collected from organs were stained with fluorescence-conjugated primary antibodies to detect cell surface markers. After surface marker detection, intracellular protein detection was required for cell fixation and permeabilization. Therefore, the cells were fixed and permeabilized using a Fixation/Permeabilization Kit (BD, Franklin Lakes, NJ, USA) and incubated with intracellular marker fluorescence antibodies. Cell marker detection was performed using a NovoCyte Flow Cytometer System (Agilent, Santa Clara, CA, USA), which allowed the detection of fluorescence signals [20].

Western blotting

To investigate protein expression levels, we used western blotting to detect protein expression in tissues. First, we lysed the tumor tissues using radioimmunoprecipitation assay (RIPA) lysis buffer (Merck, Kenilworth, NJ, USA), which contained protease and phosphatase inhibitors, to obtain the total protein extraction lysates. Total proteins were separated using 12% sodium dodecyl sulfate–polyacrylamide gel electrophoresis (SDS-PAGE) and transferred onto polyvinylidene fluoride (PVDF) membranes. The membranes were then incubated with primary and

(See figure on next page.)

Fig. 2 The biodistribution pattern of lipo-sunitinib in RCC models. **A** Lipo-sunitinib was labeled with the lipophilic tracers DiI or DiR to assess biodistribution and observation in vitro and in vivo. **B** A498 and RENCA cells were subjected to IF to evaluate the observation of DiI-labeled lipo-sunitinib. DAPI and DiI were used to represent nuclei and observed lipo-sunitinib, respectively. **C, D** Lipo-sut DiR and free DiR were intravenously injected into RCC orthotopic models, and the distribution of DiR signals was tracked over a time period of 0–48 h. **E** The primary organs were harvested for *ex vivo* detection of DiR signals to analyze the biodistribution of lipo-sut-DiR and free DiR groups (T=tumor, K=kidney, B=brain, H/LG=heart/lungs, L=livers, S=spleen). **F** The DiR signals from RCC kidneys were compared with those from normal kidneys. **G** RCC orthotopic tumors were harvested from DiI-labeled lipo-sunitinib, and DiI fluorescence signals were detected with excitation and emission wavelengths of 555 and 584 nm, respectively (T = tumor tissue, N = normal tissue). Scale bar, 100 μm

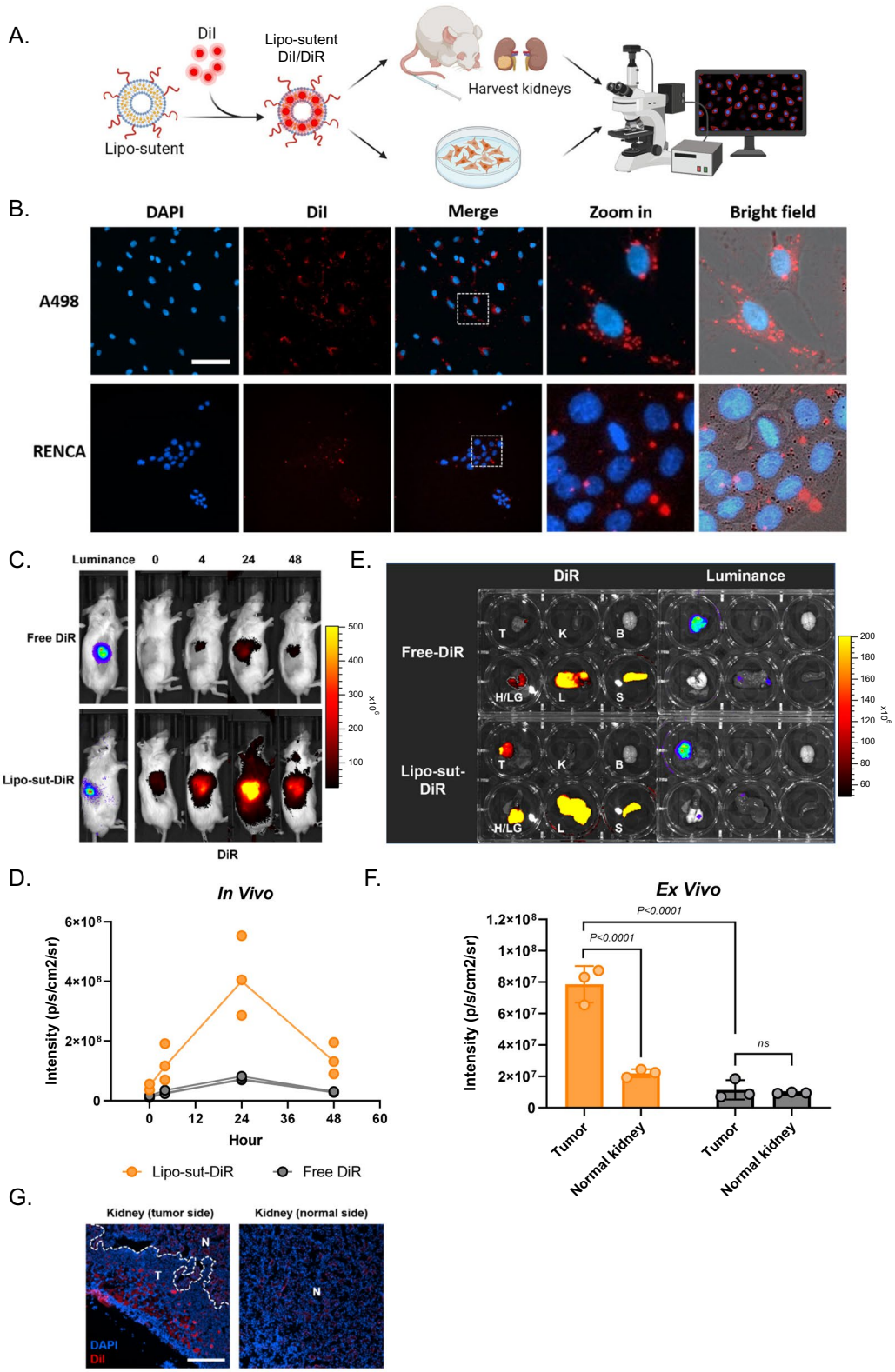

Fig. 2 (See legend on previous page.)

horseradish peroxidase-conjugated secondary antibodies to detect the proteins of interest. Proteins were visualized by performing enhanced chemiluminescence (ECL) chemical reactions to express specific band signals, which were then observed and quantified using VisionWorks (Analytik Jena, Jena, Germany) [21].

Statistical analysis

Two-way analysis of variance (ANOVA) was used to determine significant differences between groups. Statistical significance was set at $P < 0.05$. Each value in this study is displayed as the mean ± standard error. Symbols representing statistical differences between groups are mentioned in each figure legend.

Results

Preparation and characterization of lipo-sunitinib

We used an AS gradient between the liposomes and drug-containing solutions to efficiently encapsulate sunitinib into lipo-sunitinib (Fig. 1A). After optimizing the synthetic parameters, a high encapsulation efficiency of 95.7%. The molar ratio of the final lipo-sunitinib formulation was HSPC: Cholesterol (Chol): DSPE-mPEG2000 = 3:2:0.045. Lipo-sunitinib contains phospholipids (30 mM) and sunitinib (9.9 mg/mL), resulting in a drug-to-lipid ratio (of 333 mg/mmol).

Lipo-sunitinib exhibited a uniform distribution and spherical nanostructure, as revealed by TEM images taken at 2000 and 20,000× magnifications (Fig. 1B). The average hydrodynamic diameter of lipo-sunitinib was measured to be 173.4 nm with a polydispersity index (PDI) of 0.14, indicating a monodispersed size distribution (Fig. 1C). The mean zeta potential of lipo-sunitinib was observed to be −2.43 mV, suggesting that the nonionic PEG effectively shielded the surface and was expected to confer anti-fouling properties, while in circulation within the bloodstream (Fig. 1D).

Lipo-sunitinib demonstrated a pH-sensitive drug release behavior. Sunitinib was minimally released from the liposomes at pH 7.4, reaching an equilibrium plateau with only a 3.3% cumulative release (Fig. 1E). In contrast, accelerated drug release from lipo-sunitinib was observed at pH 5.5 compared to that at pH 7.4, resulting in over 42.8% cumulative release at 96 h. This behavior may be attributed to the pH-dependent solubility of sunitinib, as it exhibits high solubility in acidic aqueous solutions (25 mg mL^{-1}) but poor solubility under physiological conditions. This property enables lipo-sunitinib to maintain drug encapsulation during circulation and achieve drug release when the liposome is delivered intracellularly to endosomes or lysosomes in cancer cells, potentially enhancing its therapeutic index. To assess the safety of lipo-sunitinib in the circulatory system, we conducted a hemolysis assay to evaluate its stability in mouse whole blood (Fig. 1F). The results unequivocally demonstrated that lipo-sunitinib exhibited no hemolytic effects across a range of doses, from a low dose of 7.8 μg/mL to a high dose of 1000 μg/mL.

The biodistribution shows the accumulation pattern of lipo-sunitinib in RCC models

In theory, liposomes are expected to interact with the tumor surface and induce endocytosis to facilitate the absorption of encapsulated sunitinib by tumors. To delve deeper into this phenomenon, we used the lipophilic tracer DiI to label the bilayer phospholipids of lipo-sunitinib (Fig. 2A). Next, we exposed the human and mouse RCC cell lines, A498 and RNECA, respectively, to DiI-labeled lipo-sunitinib for 4 h. The results demonstrated the substantial and targeted absorption of DiI-labeled lipo-sunitinib in RCC cells (Fig. 2B).

To further examine the in vivo biodistribution of lipo-sunitinib, we employed a similar fluorescence-labeling method. DiR lipophilic tracer-labeled lipo-sunitinib was injected into the RCC orthotopic models, and the DiR signal was monitored over a 48-h time lapse (Fig. 2C). The DiR signal exhibited the highest colocalization with orthotopic tumors at the 24-h mark (Fig. 2D). After 48 h, various organs and orthotopic tumors were isolated for DiR signal analysis (Fig. 2E). Notably, the DiR signal in the primary tumor of the lipo-sunitinib group was higher

(See figure on next page.)

Fig. 3 Lipo-sunitinib strongly upregulates cytotoxicity through autophagy induction in RCC. **A**, **B** MTT assays were conducted to compare the cytotoxicity of sunitinib and lipo-sunitinib in RENCA and A498 cell lines. **C** RENCA cells treated with lipo-sunitinib underwent RNA-seq analysis, revealing significantly upregulated pathways compared to the non-treated group. **D** RNA-seq data for lipo-sunitinib were subjected to GSEA analysis with a focus on macrophagy and autophagosome pathways. **E** IF analysis of RENCA and A498 cells included detection of LC3B and p62 expression using GFP and RFP channels, with DAPI staining representing nuclei. **F** In addition, LC3B protein expression in RENCA and A498 cells were assessed using western blotting assays. **G** The subcutaneous RCC xenograft models were constructed using BALB/c mice with RENCA cells subcutaneously injection. Vehicle and sunitinib groups were administrated 0.1% DMSO and 30 mg/kg sunitinib through daily gavage, respectively, and the **H** tumor volume of RCC was measured twice daily. Mice are sacrificed on day 14, and all tumors were isolated from mice for **I** weighting and **J** imaging. **K** Body weights of mice were also measured twice daily after treatment started. **L** Several organs of the subcutaneous RCC xenograft model (liver, heart, and kidneys) were subjected to H&E staining. Scale bar, 50 μm

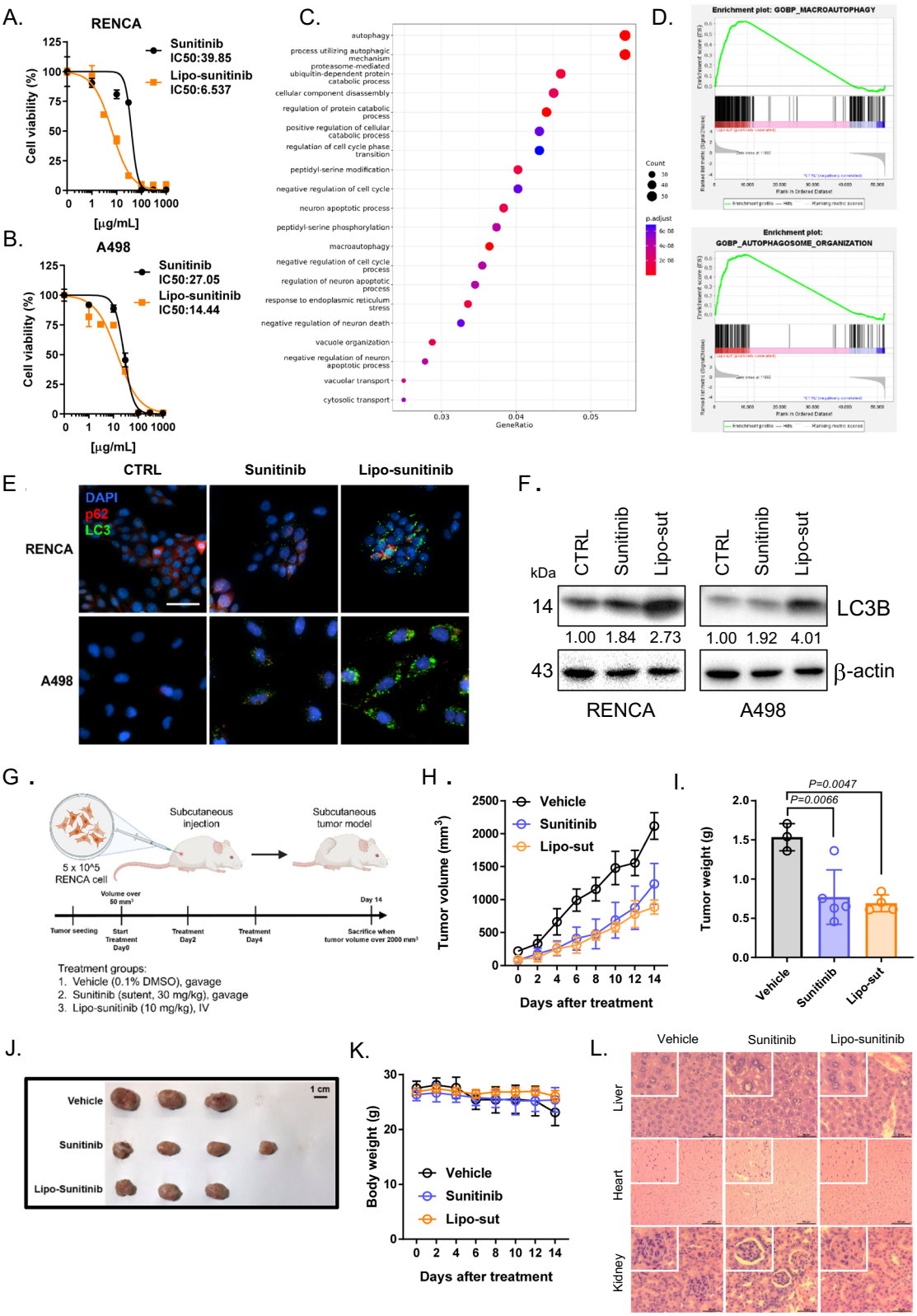

Fig. 3 (See legend on previous page.)

than that in the non-tumor kidney tissue and primary tumor of the free DiR group (Fig. 2F).

For in vivo fluorescence to validate the distribution of lipo-sunitinib in vivo, DiI-labeled lipo-sunitinib was injected into RCC orthotopic models and collected from the kidneys (tumor and non-tumor sides) for fluorescence observation (Fig. 2A). We observed that tumor tissues from the RCC orthotopic models had DiI signal accumulation, and no signals were observed in normal tissues (Fig. 2G). These results indicate that the absorption and distribution of lipo-sunitinib can be observed both in vitro and in vivo.

Lipo-sunitinib strongly upregulate cytotoxicity through autophagy induction in RCC

We hypothesized that liposomes may deliver more sunitinib into cells to induce stronger cell death. The cell viability assay showed that lipo-sunitinib induced cell death at lower drug concentrations in both RENCA and A498 cells (Fig. 3A and B). To further investigate this mechanism, we performed RNA-seq on RENCA cells after lipo-sunitinib treatment. The results indicated that lipo-sunitinib significantly upregulated autophagy and related pathways in RNA-seq (Fig. 3C) and GSEA analyses (Fig. 3D). To further investigate this, we used IF and immunoblotting (IB) to determine the expression of the autophagy-related proteins LC3B and p62. LC3B plays a crucial role in the formation of autophagosomes and double-membrane vesicles that sequester cellular components targeted for degradation, whereas p62 is also involved in autophagosome formation. These results indicated that sunitinib and lipo-sunitinib induced autophagy through LC3B and p62 expression and colocalization (Fig. 3E), and lipo-sunitinib induced greater autophagosome formation than sunitinib (Fig. 3F).

These results show that lipo-sunitinib may deliver more suitable molecules into RCC cells, inducing stronger cytotoxicity through autophagy upregulation. According to these studies, despite the high therapeutic efficacy of sunitinib in patients with advanced RCC, sunitinib has several unexpected side effects. Therefore, we first verified the safety and efficacy of lipo-sunitinib in murine and human RCC subcutaneous xenograft models, including both RECNA- and A498-bearing models. (Fig. 3G). In the subcutaneous injection model, lipo-sunitinib (10 mg/kg) was administered at a lower dose than sunitinib (30 mg/kg). The tumor volumes and weights showed no significant differences between lipo-sunitinib and sunitinib treatments, but markedly reduced as compare to control group (Fig. 3H–J, Supplementary Figures S1A and C). In addition, we evaluated LC3B expression in tumor tissue sections, which showed increased autophagy (Supplementary Figures S2A and B).

In the general toxicity test, neither sunitinib nor lipo-sunitinib groups showed acute toxicity in mouse body weight measurements (Fig. 3K and Supplementary Figure S1B). However, the liver, heart, and kidney tissues showed different levels of damage from sunitinib, which was not observed with lipo-sunitinib (Fig. 3L, Supplementary Figure S1G). Serological tests of mouse plasma were conducted to validate the toxicity of lipo-sunitinib and sunitinib. We measured creatinine (CREA) levels for kidney damage, lactate dehydrogenase (LDH) levels for general tissue damage, and aspartate transaminase (AST) and alanine transaminase (ALT) levels for liver damage (Supplementary Figure S1D-F). These results indicate that lipo-sunitinib did not cause general tissue damage. The results indicated that lipo-sunitinib can achieve the same efficacy as sunitinib in inhibiting tumor growth, along with higher safety and lower dosage.

Lipo-sunitinib inhibits the tumor metastasis and prolong the RCC model survival

We investigated the potential of lipo-sunitinib to achieve superior therapeutic efficacy in the treatment of RCC compared with conventional sunitinib. To assess this, we established a traceable luminescent RCC cell line (RENCA/luc) and implanted it into the left kidney of BALB/c mice. The experimental groups were randomly assigned and treated with the sutent via both oral and intravenous (IV) administration, whereas lipo-sunitinib was administered exclusively via IV (Fig. 4A). To ensure an equitable efficacy assessment, we maintained uniform treatment dosages across all groups.

(See figure on next page.)

Fig. 4 Lipo-sunitinib inhibits tumor metastasis and prolongs the survival of RCC model mice. **A** RCC orthotopic models were established in BALB/c mice by injecting RENCA/luc cells into the left kidneys. The vehicle and oral-sut groups received 0.1% DMSO and 10 mg/kg sunitinib through gavage thrice weekly, whereas the IV-sut and lipo-sunitinib groups were administered 10 mg/kg of sunitinib and lipo-sunitinib by IV injection thrice weekly. **B** Bioluminescence imaging was performed weekly to monitor RCC tumor progression, and **C** the quantification panel was statistically analyzed based on photon counts. **D** After sacrificing the mice, the left kidneys (containing the RCC tumor) were isolated for imaging. **E** The survival rate of RCC orthotopic models was analyzed, and **F** lung tissues were isolated to detect metastasis through imaging. **G** RNA-seq data for lipo-sunitinib were subjected to GSEA analysis, with a specific focus on EMT pathways. **H** mRNA expressions related to EMT pathways were further analyzed based on the GSEA results

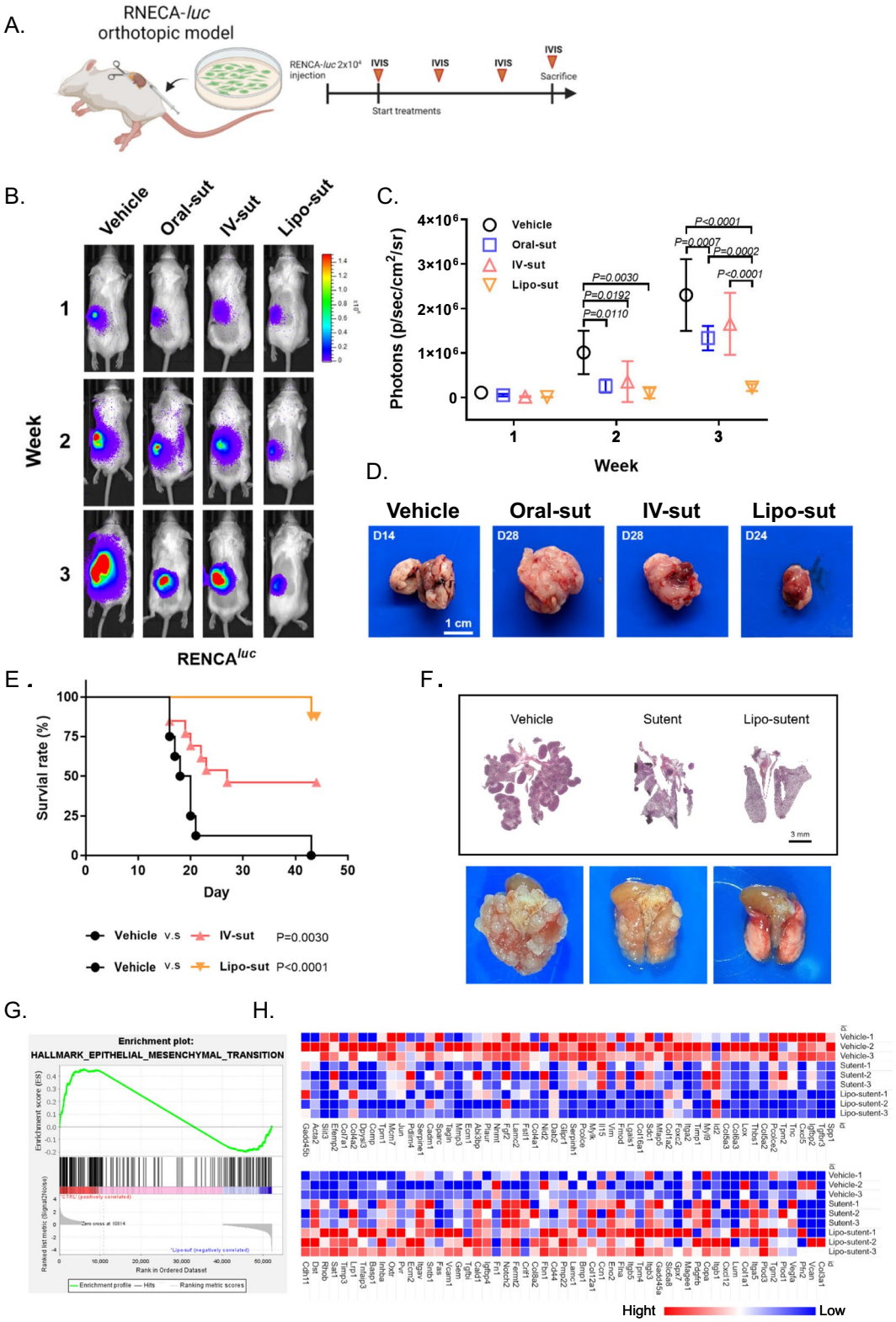

Fig. 4 (See legend on previous page.)

Bioluminescence images (Fig. 4B) showed the progression of RCC, revealing significantly lower luminescence signals for lipo-sunitinib (Lipo-sut) than for oral and IV sunitinib (Oral-sut and IV-sut, respectively) administration (Fig. 4C). These findings strongly suggested that liposomal-encapsulated sunitinib exhibited superior therapeutic efficacy compared to conventional oral and IV sunitinib administration (Fig. 4D).

Moreover, lipo-sunitinib treatment demonstrated the highest survival rate (Fig. 4E) compared to IV-sut treatment. Interestingly, post-sacrifice observations revealed lung metastasis and strong angiogenesis in both the vehicle and IV-sut groups (Fig. 4F, Supplementary Figure S3A). This observation aligns with the RNA-seq results, as pathway analysis indicated a downregulation of EMT and angiogenesis in lipo-sunitinib treatment compared to vehicle treatment (Fig. 4G, Supplementary Figure S3B). mRNA expression analysis further confirmed the strong effect of lipo-sunitinib treatment on EMT-related genes (Fig. 4H). Metastasis markers, such as Snail-1 and Vimentin, decreased after lipo-sunitinib treatment in human RCC tumor models (Supplementary Figure S2B). Overall, lipo-sunitinib prolonged orthotopic survival in patients with RCC and inhibited lung metastasis by downregulating the EMT pathway.

The lipo-sunitinib significantly modulates the RCC TME

The TME plays a critical role in influencing both the direct and indirect aspects of tumor progression. Therefore, investigation of whether lipo-sunitinib can modulate RCC TME is important. In our analysis, we initially examined multiple immune-related pathways, including immune response regulation, antigen processing, and cytokine production, in RENCA cells treated with lipo-sunitinib (Supplementary Figure S4). Antigen presentation and cytokine production are pivotal pathways that stimulate anticancer efficacy. mRNA expression analysis revealed that lipo-sunitinib significantly upregulated antigen processing, cytokine production, and lymphocyte chemotaxis compared to conventional sunitinib (Fig. 5A). These findings suggest that RCC tumors treated with lipo-sunitinib may attract anticancer immune cell infiltration (via cytokine production) and stimulate T cell activity (via antigen processing).

To further investigate immune modulation, we collected tumor tissues and performed staining for activated cytotoxic T cells ($CD8^+IL\text{-}2^+IFN\text{-}\gamma^+$ Teffs) and activated dendritic cells ($CD11c^+MHCII^+$ dendritic cells [DCs]) (Fig. 5B). The results demonstrated that lipo-sunitinib had the highest Teff infiltration among the groups, whereas DCs infiltration was comparable within the oral-sut, IV-sut, and lipo-sut groups. Flow cytometry was used to assess the infiltration of Teffs and immunosuppressive regulatory T cells ($CD4^+CD25^+Foxp3^+$ Tregs). The data revealed that lipo-sunitinib significantly increased anticancer Teffs and decreased Treg infiltration compared with vehicle, oral-sut, and IV-sut (Fig. 5C).

Furthermore, we isolated RCC cells from the entire tumor tissue and examined PD-L1 expression by flow cytometry and western blotting (Fig. 5D). PD-L1 expression was markedly reduced in the lipo-sunitinib group compared to that in the sunitinib group. In addition, the level of the apoptosis marker cleaved caspase-3 increased in the lipo-sunitinib group (Fig. 5D). The expression level of PD-L1 in tumor tissue assayed by flow cytometry was also markedly decreased by lipo-sunitinib (Fig. 5E). These results suggest that lipo-sunitinib significantly modulates the RCC TME by upregulating antigen processing and chemotaxis, leading to increased infiltration and activation of anticancer immune cells such as cytotoxic T cells and DCs.

The lipo-sunitinib affects systemic anti-*cancer* immunity in RCC model

In the field of immuno-oncology, maintaining robust systemic immunity is crucial for effective immune surveillance and tumor suppression. Consequently, we conducted a comprehensive validation of the expression of various immune cells across different tissues, including the tumor-draining lymph nodes (TDLN), spleen, and bone marrow, using flow cytometry. Our findings revealed that lipo-sunitinib treatment resulted in a notable increase in the population of Teffs, type 1 dendritic cells ($CD11c^+CD24^+MHCII^+$ cDC1), and memory effector T cells ($CD8^+CD44^+CD62L^{low}$ Tem) within the

(See figure on next page.)

Fig. 5 Lipo-sunitinib significantly modulates the RCC TME. **A** RNA-seq was performed to analyze the mRNA expression of antigen processing and presentation, cytokine production, and lymphocyte chemotaxis pathways. **B** The left kidneys (orthotopic tumor) were subjected to cryosection for IF staining. For active effector T cell staining, tumors were stained with CD8 and IFN-γ, then DCs were stained with CD11c and MHCII. **C** The TIL in RCC tumor tissue was measured using fluorescence-antibody analysis and verified using flow cytometry. Active effector T cells in TIL were stained for CD8, IL-2, and IFN-γ. Tregs were stained for CD4, CD25, and Foxp3. **D** Subcutaneous RCC tumors were collected for protein extraction, and tumor PD-L1 expression was analyzed using estern blotting. **E** Immune checkpoint PD-L1 on tumor cells was stained with the anti-PD-L1 fluorescence antibody

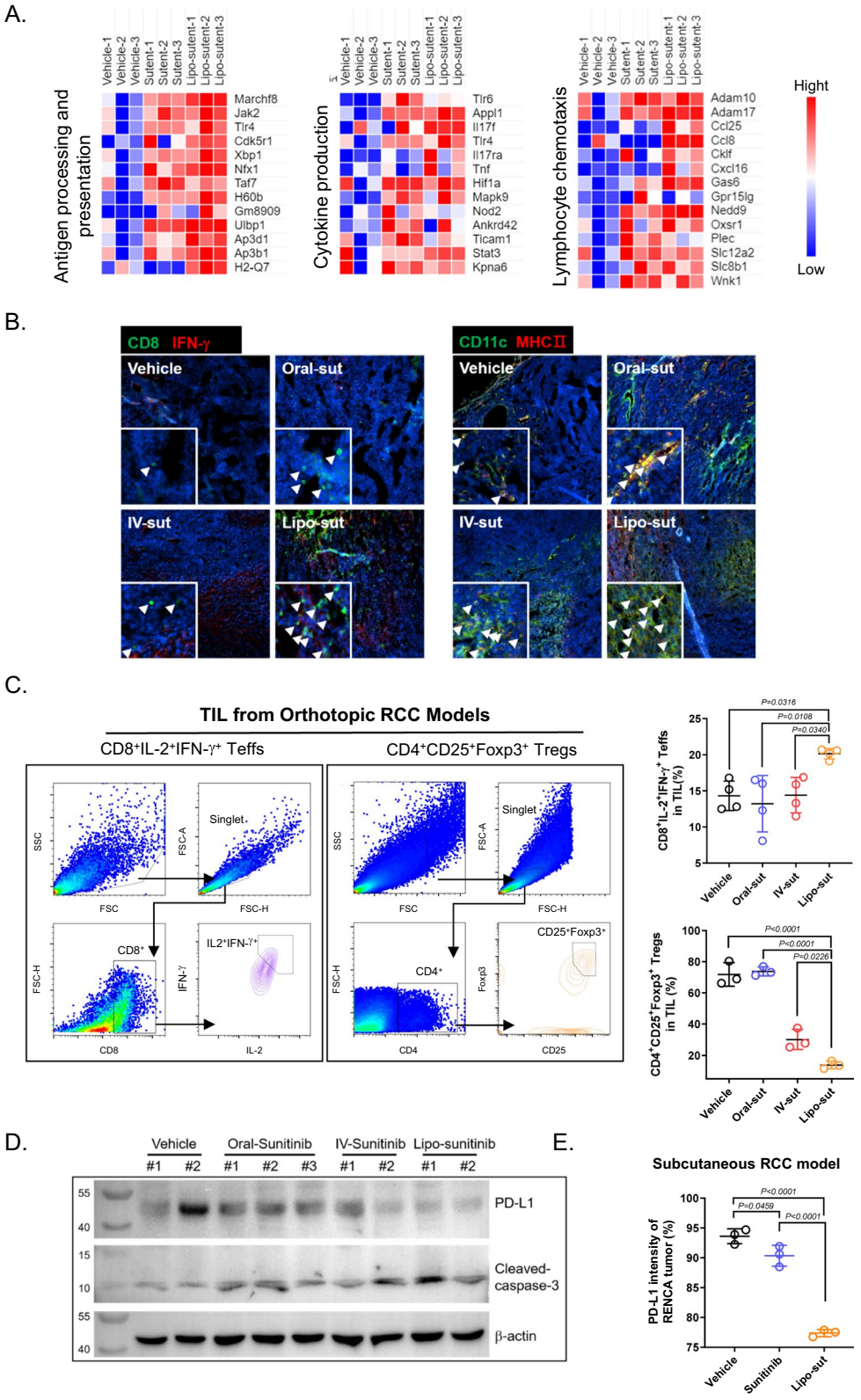

Fig. 5 (See legend on previous page.)

TDLN of the orthotopic RCC models (Fig. 6A). In addition, lipo-sunitinib treatment led to a decrease in the TDLN's population of Tregs (Supplementary Figure S5). Combining these results with those of TIL from RCC tumors, it became evident that lipo-sunitinib may stimulate DCs to migrate back into TDLN, thereby educating naïve T cells into Teffs and Tems.

Similarly, in comparison with the oral-sut and IV-sut groups, lipo-sunitinib treatment resulted in an augmented population of Teffs and cDC1 coupled with a decreased population of Tregs in the spleen of orthotopic RCC models (Fig. 6B). Examining the bone marrow, we observed a significant reduction in myeloid-derived suppressive macrophages ($CD11b^{+}Gr\text{-}1^{+}$ MDSCs) within the lipo-sunitinib group compared to that in the oral-sut and IV-sut groups (Fig. 6C). In summary, our results suggest that lipo-sunitinib influences RCC tumor cytotoxicity through autophagy induction, angiogenesis inhibition, and EMT inhibition and also modulates anti-cancer immunity by enhancing both local and systemic immune responses.

Discussion

Several studies have highlighted the use of sunitinib as a dual drug. Its potent tumor inhibition, as a multiple tyrosine kinase inhibitor, has led to FDA approval for the treatment of patients with advanced RCC [4, 5]. However, it also triggers significant adverse effects stemming from its general toxicity. In the history of drug delivery, liposomes have proven to be a stable and efficient method for delivering small molecules into human cells [22, 23]. Successful clinical cases, such as Liposomal doxorubicin (Myocet), Liposomal daunorubicin (Daunoxome), and Stealth (PEGylated) liposomal doxorubicin (Doxil™/Caelyx), underscore the efficacy of liposomal chemotherapy drugs [12, 24–27]. Notably, the Moderna SARS-CoV-2 mRNA vaccine uses liposomes to encapsulate mRNA for gene delivery, affirming the safety and feasibility of this approach [28].

Given this evidence, our objective was to develop a liposome-based, easily synthesizable, and safe vehicle for delivering lipo-sunitinib nanoparticles and to assess its anticancer efficacy and underlying mechanism. Our liposomes, obtained through the emulsification method (Fig. 1A), had surfaces modified by PEGylation, resulting in a diameter of approximately 100 nm (Fig. 1C) and electrical neutrality (Fig. 1D) due to PEG modification [16]. A larger particle size may extend the half-life of lipo-sunitinib in the circulatory system. Furthermore, owing to its nanoscale characteristics, it can selectively and passively target tumor tissues through the enhanced permeability and retention (EPR) effect. This phenomenon is facilitated by the normalization of tumor vessels, which results in the leakage and infiltration of nanoscale particles. Hence, our initial focus was to evaluate the biodistribution pattern of lipo-sunitinib both in vitro and in vivo. By leveraging the distinctive properties of DiI and DiR, these dyes were readily incorporated into the bilayer phospholipid structure of lipo-sunitinib (Fig. 2A). This feature allowed us to monitor the distribution of lipo-sunitinib in orthotopic RENCA RCC tumor models. Our findings demonstrated that lipo-sunitinib efficiently and rapidly permeated the orthotopic RCC implantation site in the kidneys (Fig. 2F and G) [29]. Consequently, our results suggested that lipo-sunitinib is an effective means of delivering therapeutic agents to tumor sites. Notably, even at reduced concentrations, this approach achieved comparable tumor inhibition results (Fig. 3H-K and Supplementary Figure S1).

A recent study showed that sunitinib has the capacity to diminish PD-L1 expression in RCC cells by inducing autophagy, thereby enhancing anti-cancer immunity within the TME [7]. This concept opens up two intriguing avenues for exploration: one involving a heightened autophagic response indicative of cell death and growth inhibition [30–32], and the other pointing toward more robust immune modulation [33, 34]. To elucidate the underlying mechanisms, we conducted RNA-seq analyses on RENCA cells treated with vehicle, sunitinib, or lipo-sunitinib. As anticipated, lipo-sunitinib induced a greater level of autophagy than both the vehicle and sunitinib treatments (Fig. 3C–F). Interestingly, our investigation revealed that the RCC orthotopic model exhibited strong lung metastasis and that both sunitinib and lipo-sunitinib effectively curtailed this metastatic process

(See figure on next page.)

Fig. 6 The systemic immunology modulation effect of lipo-sunitinib in RCC orthotopic model mice. After RCC-bearing mice were sacrificed, immune organs, including the TDLN, spleen, and bone marrow, were collected for immune modulation testing using flow cytometry. **A** In TDLN cells, staining with CD8, IL-2, and IFN-γ represented Teffs, whereas staining with CD11c, CD24, and MHCII represented cDC1. In addition, staining with CD8, CD44, and CD62 represented Tem, and staining with CD4, CD25, and Foxp3 represented Tregs. **B** Splenocytes from RCC-bearing mice spleen were collected and stained for CD8, IL-2, and IFN-γ represented Teffs, whereas staining for CD11c, CD24, and MHCII represented cDC1. Moreover, staining for CD4, CD25, and Foxp3 represented Tregs. **C** Bone marrow collected from the thigh bone of RCC-bearing mice was analyzed, and staining for CD11b and Gr-1 was indicative of MDSCs

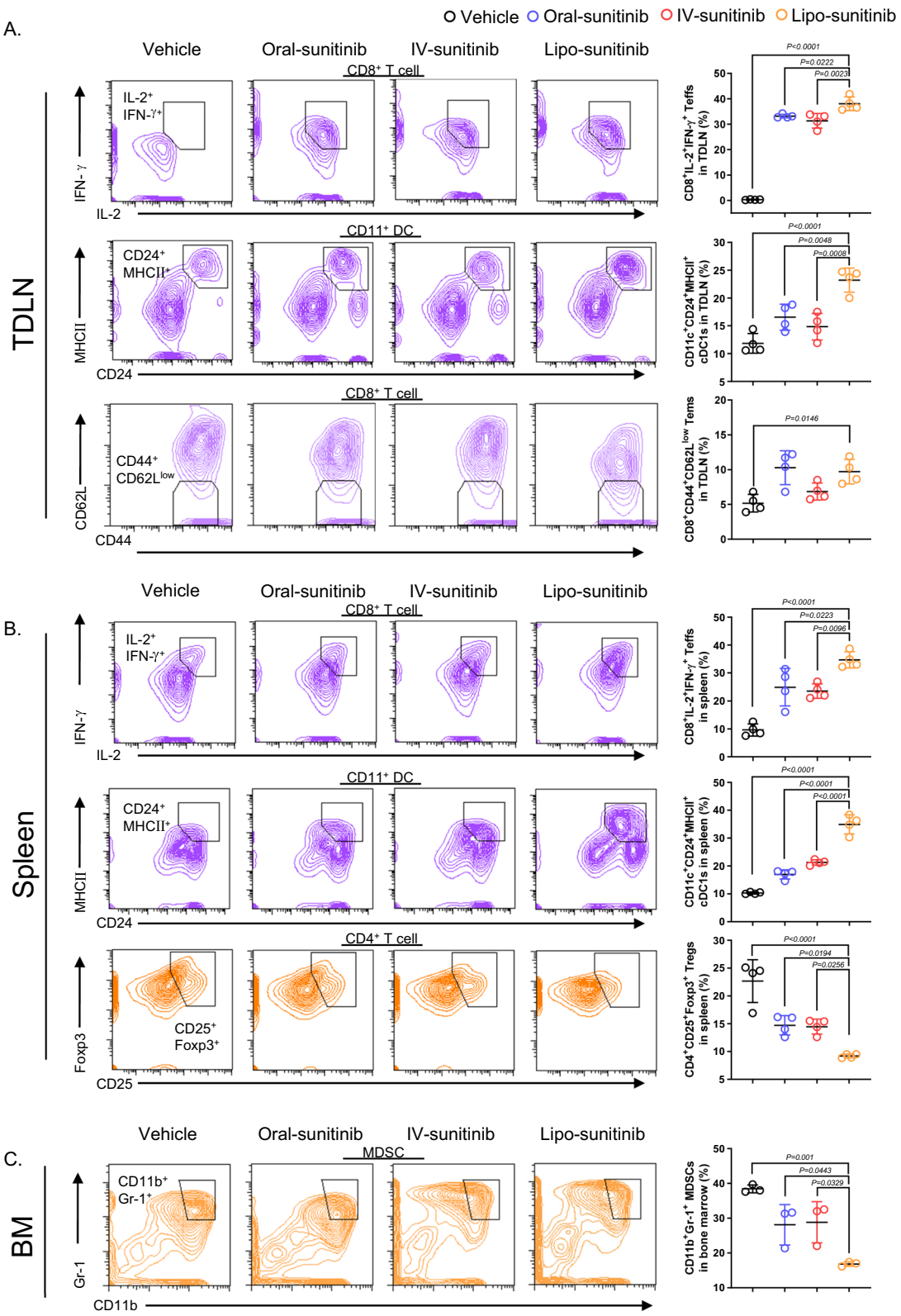

Fig. 6 (See legend on previous page.)

(Fig. 4F). Consequently, we analyzed RNA-seq data, revealing that lipo-sunitinib significantly downregulated the EMT pathway in RENCA cells (Fig. 4G and H), an important factor associated with tumor metastasis [35–38]. This may be one reason why lipo-sunitinib significantly prolonged the survival rate of orthotopic models.

Upon analyzing the RNA-seq data, we observed that processes such as antigen processing and presentation, cytokine production, and lymphocyte chemotaxis were upregulated in RENCA cells following treatment with lipo-sunitinib. Although these changes did not reach statistical significance in the GSEA, certain crucial genes were significantly upregulated. Notably, our findings highlight that lipo-sunitinib has the potential to enhance antigen presentation on the cell surface, thereby fostering the activation of anticancer immune cells such as effector T cells through antigen recognition. Moreover, the upregulation of chemotaxis (CCL25, CCL8, CXCL16) implies that RCC cells treated with lipo-sunitinib have an increased capacity to attract immune cell infiltration, transforming the microenvironment into a "hot" tumor [39, 40]. This immune-active setting is conducive for combination treatments involving immune checkpoint inhibitors.

To explore immune modulation induced by lipo-sunitinib treatment in vivo, we established immunocompetent orthotopic mice with RCC and administered sunitinib and lipo-sunitinib (Fig. 4A). Our initial focus was on tumor cells and tumor-infiltrating lymphocytes (TILs). The results demonstrated that lipo-sunitinib treatment increased the percentage of active $CD8^+$ T cells, which was consistent with the transcriptomic findings (Fig. 5B and C). Simultaneously, the presence of $CD11c^+$ $MHCII^+$ dendritic cells within TILs increased (Fig. 5B), suggesting that RCC tumors may attract immune cell migration to the tumor site through cytokine and chemokine production. To further assess this effect, we subcutaneously implanted RENCA cells into immunocompetent mice and treated them with sunitinib and lipo-sunitinib to observe PD-L1 expression. As expected, both the sunitinib and lipo-sunitinib groups exhibited greater downregulation of PD-L1 expression than the sunitinib-only group. Our findings corroborate existing studies as well as reveal additional potential immune modulation pathways associated with lipo-sunitinib treatment.

Finally, we examined the systemic immune organs and tissues to assess whether lipo-sunitinib can influence the broader landscape of adaptive immune modulation. TDLN have particular significance as they significantly impact the anticancer immune response [41–43]. When cDC1 is attracted by chemokines secreted by tumor tissue, it engages in phagocytosis to acquire tumor antigens [44–46]. Subsequently, cDC1 migrates back into the TDLN, stimulating naïve T cells to recognize the tumor cells. In line with this concept, our results demonstrated that the number of effector T cells, cDC1, and memory effector T cells increased after lipo-sunitinib treatment in orthotopic RCC models (Fig. 6A). Moreover, less prominent organs, such as the spleen and bone marrow, also exhibit positive effects on anti-cancer immune modulation. This included an increase in effector T cells and cDC1 in the spleen, along with a decrease in Tregs in the spleen and MDSCs in the bone marrow (Fig. 6B and C).

In our study, we successfully and efficiently delivered sunitinib to RCC tumors using PEGylated liposomes, without inducing toxicity. In comparison with other studies, we observed similar findings of autophagy induction and decreased PD-L1 expression in RCC cells. Next, we performed RNA-seq analysis to examine the transcriptomic landscape and identify potential mechanisms. Significantly, we observed a downregulation of the EMT pathway, a key player in metastasis, following lipo-sunitinib treatment. Moreover, lipo-sunitinib influenced antigen presentation and chemokine production in RCC tumors, thereby orchestrating a comprehensive shift toward an immunogenic TME. These results suggest that lipo-sunitinib has the potential to synergize with immune checkpoint inhibitors in the treatment of patients with advanced RCC, providing them with innovative therapeutic options and strategies.

Conclusions

We observed that lipo-sunitinib infiltrated the RCC tumor site, concurrently inducing potent autophagy, elevating antigen presentation, activating cytokine and chemokine production pathways, and downregulating EMT in RCC cells. This comprehensive approach significantly enhances tumor inhibition and fosters anticancer immune modulation, thereby presenting patients with innovative therapeutic options and strategic interventions.

Supplementary Information

The online version contains supplementary material available at https://doi.org/10.1186/s12951-024-02664-5.

Supplementary Material 1.

Acknowledgements

Experiments and data analysis were partially conducted at the Medical Research Core Facilities Center, Office of Research & Development, China Medical University, Taichung, Taiwan, ROC. The study received support from the National Science and Technology Council, Taipei, Taiwan (ID: NSTC 112-2314-B-039-063 -MY3 and 112-2926-I-039-501-G) and China Medical University, Taichung, Taiwan (ID: CMU112-MF-53).

Author contributions
Experiments and data analysis were conducted by PFY, CSC, IJT, and FTH, with contributions to manuscript drafting. Validation was carried out by PFY, CSC, IJT, YLT, HRC and FTH. Methodological and software support were provided by CSC, YLT, HRC and KLL. PFY, KLL, and FTH conceptualized the research, provided supervision, secured funding, oversaw the project, and completed the manuscript.

Data availability
No datasets were generated or analysed during the current study.

Declarations

Competing interests
The authors declare no competing interests.

Author details
[1]Institute of Traditional Medicine, National Yang Ming Chiao Tung University, 6th Floor, Shouren Building, No. 155, Section 2, Linong Street, Beitou District, Taipei 112, Taiwan, ROC. [2]Graduate Institute of Biomedical Sciences, China Medical University, Taichung, Taiwan, ROC. [3]Cell Therapy Center, China Medical University Hospital, Taichung, Taiwan, ROC. [4]Taiwan Liposome Company, Ltd., Taipei, Taiwan, ROC. [5]Department of Heavy Ion and Radiation Oncology, Taipei Veterans General Hospital, Taipei, Taiwan. [6]Department of Biology Science and Technology, China Medical University, 7F, Research Building, No. 100, Jingmao 1st Rd., Beitun Dist., Taichung City 406, Taiwan, ROC. [7] Department of Heavy Particles & Radiation Oncology, Taipei Veterans General Hospital, Taipei, Taiwan.

Received: 26 January 2024 Accepted: 24 June 2024
Published online: 31 July 2024

References

1. Turajlic S, Swanton C, Boshoff C. Kidney cancer: the next decade. J Exp Med. 2018;215:2477–9.
2. Rini BI, Campbell SC, Escudier B. Renal cell carcinoma. Lancet. 2009;373:1119–32.
3. Barata PC, Rini BI. Treatment of renal cell carcinoma: current status and future directions. CA Cancer J Clin. 2017;67:507–24.
4. Schmid TA, Gore ME. Sunitinib in the treatment of metastatic renal cell carcinoma. Ther Adv Urol. 2016;8:348–71.
5. Pan Y, Lu X, Shu G, Cen J, Lu J, Zhou M, Huang K, Dong J, Li J, Lin H, et al. Extracellular vesicle-mediated transfer of LncRNA IGFL2-AS1 confers sunitinib resistance in renal cell carcinoma. Cancer Res. 2023;83:103–16.
6. Papaetis GS, Syrigos KN. Sunitinib: a multitargeted receptor tyrosine kinase inhibitor in the era of molecular cancer therapies. BioDrugs. 2009;23:377–89.
7. Li H, Kuang X, Liang L, Ye Y, Zhang Y, Li J, Ma F, Tao J, Lei G, Zhao S, et al. The beneficial role of sunitinib in tumor immune surveillance by regulating tumor PD-L1. Adv Sci. 2021;8:2001596.
8. Chu TF, Rupnick MA, Kerkela R, Dallabrida SM, Zurakowski D, Nguyen L, Woulfe K, Pravda E, Cassiola F, Desai J, et al. Cardiotoxicity associated with tyrosine kinase inhibitor sunitinib. Lancet. 2007;370:2011–9.
9. Gupta R, Maitland ML. Sunitinib, hypertension, and heart failure: a model for kinase inhibitor-mediated cardiotoxicity. Curr Hypertens Rep. 2011;13:430–5.
10. Shi Y, van der Meel R, Chen X, Lammers T. The EPR effect and beyond: strategies to improve tumor targeting and cancer nanomedicine treatment efficacy. Theranostics. 2020;10:7921–4.
11. Ikeda-Imafuku M, Wang LL, Rodrigues D, Shaha S, Zhao Z, Mitragotri S. Strategies to improve the EPR effect: a mechanistic perspective and clinical translation. J Control Release. 2022;345:512–36.
12. Barenholz Y. Doxil®–the first FDA-approved nano-drug: lessons learned. J Control Release. 2012;160:117–34.
13. Allen TM, Cullis PR. Liposomal drug delivery systems: from concept to clinical applications. Adv Drug Deliv Rev. 2013;65:36–48.
14. Gabizon A, Shmeeda H, Barenholz Y. Pharmacokinetics of pegylated liposomal Doxorubicin: review of animal and human studies. Clin Pharmacokinet. 2003;42:419–36.
15. Gabizon A, Martin F. Polyethylene glycol-coated (pegylated) liposomal doxorubicin. Rationale for use in solid tumours. Drugs. 1997;54(Suppl 4):15–21.
16. Yuan W, Kuai R, Dai Z, Yuan Y, Zheng N, Jiang W, Noble C, Hayes M, Szoka FC, Schwendeman A. Development of a flow-through USP-4 apparatus drug release assay to evaluate doxorubicin liposomes. Aaps J. 2017;19:150–60.
17. Sæbø IP, Bjørås M, Franzyk H, Helgesen E, Booth JA. Optimization of the hemolysis assay for the assessment of cytotoxicity. Int J Mol Sci. 2023;24(3):2914.
18. Yueh PF, Lee YH, Chiang IT, Chen WT, Lan KL, Chen CH, Hsu FT. Suppression of EGFR/PKC-δ/NF-κB signaling associated with imipramine-inhibited progression of non-small cell lung cancer. Front Oncol. 2021;11: 735183.
19. Mirzaaghasi A, Han Y, Ahn SH, Choi C, Park JH. Biodistribution and pharmacokinectics of liposomes and exosomes in a mouse model of sepsis. Pharmaceutics. 2021;13(3):427.
20. Chiang IT, Lee YH, Tan ZL, Hsu FT, Tu HF. Regorafenib enhances antitumor immune efficacy of anti-PD-L1 immunotherapy on oral squamous cell carcinoma. Biomed Pharmacother. 2022;147: 112661.
21. Yueh PF, Lee YH, Fu CY, Tung CB, Hsu FT, Lan KL. Magnolol induces the extrinsic/intrinsic apoptosis pathways and inhibits STAT3 signaling-mediated invasion of glioblastoma cells. Life. 2021;11(12):1399.
22. Large DE, Abdelmessih RG, Fink EA, Auguste DT. Liposome composition in drug delivery design, synthesis, characterization, and clinical application. Adv Drug Deliv Rev. 2021;176: 113851.
23. Cheng X, Gao J, Ding Y, Lu Y, Wei Q, Cui D, Fan J, Li X, Zhu E, Lu Y, et al. Multi-functional liposome: a powerful theranostic nano-platform enhancing photodynamic therapy. Adv Sci. 2021;8: e2100876.
24. Duggan ST, Keating GM. Pegylated liposomal doxorubicin: a review of its use in metastatic breast cancer, ovarian cancer, multiple myeloma and AIDS-related Kaposi's sarcoma. Drugs. 2011;71:2531–58.
25. Li XR, Cheng XH, Zhang GN, Wang XX, Huang JM. Cardiac safety analysis of first-line chemotherapy drug pegylated liposomal doxorubicin in ovarian cancer. J Ovarian Res. 2022;15:96.
26. Batist G, Barton J, Chaikin P, Swenson C, Welles L. Myocet (liposome-encapsulated doxorubicin citrate): a new approach in breast cancer therapy. Expert Opin Pharmacother. 2002;3:1739–51.
27. Russo D, Piccaluga PP, Michieli M, Michelutti T, Visani G, Gugliotta L, Bonini A, Pierri I, Gobbi M, Tiribelli M, et al. Liposomal daunorubicin (DaunoXome) for treatment of poor-risk acute leukemia. Ann Hematol. 2002;81:462–6.
28. Corbett KS, Edwards DK, Leist SR, Abiona OM, Boyoglu-Barnum S, Gillespie RA, Himansu S, Schäfer A, Ziwawo CT, DiPiazza AT, et al. SARS-CoV-2 mRNA vaccine design enabled by prototype pathogen preparedness. Nature. 2020;586:567–71.
29. Forssen EA, Malé-Brune R, Adler-Moore JP, Lee MJ, Schmidt PG, Krasieva TB, Shimizu S, Tromberg BJ. Fluorescence imaging studies for the disposition of daunorubicin liposomes (DaunoXome) within tumor tissue. Cancer Res. 1996;56:2066–75.
30. Zhou B, Liu J, Kang R, Klionsky DJ, Kroemer G, Tang D. Ferroptosis is a type of autophagy-dependent cell death. Semin Cancer Biol. 2020;66:89–100.
31. Park E, Chung SW. ROS-mediated autophagy increases intracellular iron levels and ferroptosis by ferritin and transferrin receptor regulation. Cell Death Dis. 2019;10:822.
32. Liu S, Yao S, Yang H, Liu S, Wang Y. Autophagy: regulator of cell death. Cell Death Dis. 2023;14:648.
33. Ozao-Choy J, Ma G, Kao J, Wang GX, Meseck M, Sung M, Schwartz M, Divino CM, Pan PY, Chen SH. The novel role of tyrosine kinase inhibitor in the reversal of immune suppression and modulation of tumor microenvironment for immune-based cancer therapies. Cancer Res. 2009;69:2514–22.
34. Tsukita Y, Okazaki T, Ebihara S, Komatsu R, Nihei M, Kobayashi M, Hirano T, Sugiura H, Tamada T, Tanaka N, et al. Beneficial effects of sunitinib on tumor microenvironment and immunotherapy targeting death receptor5. Oncoimmunology. 2019;8: e1543526.
35. Pastushenko I, Blanpain C. EMT transition states during tumor progression and metastasis. Trends Cell Biol. 2019;29:212–26.

36. Zhang S, Hong Z, Chai Y, Liu Z, Du Y, Li Q, Liu Q. CSN5 promotes renal cell carcinoma metastasis and EMT by inhibiting ZEB1 degradation. Biochem Biophys Res Commun. 2017;488:101–8.
37. Fiori ME, Di Franco S, Villanova L, Bianca P, Stassi G, De Maria R. Cancer-associated fibroblasts as abettors of tumor progression at the crossroads of EMT and therapy resistance. Mol Cancer. 2019;18:70.
38. Yang Z, Xie H, He D, Li L. Infiltrating macrophages increase RCC epithelial mesenchymal transition (EMT) and stem cell-like populations via AKT and mTOR signaling. Oncotarget. 2016;7:44478–91.
39. Garrido-Martin EM, Mellows TWP, Clarke J, Ganesan AP, Wood O, Cazaly A, Seumois G, Chee SJ, Alzetani A, King EV, et al. M1(hot) tumor-associated macrophages boost tissue-resident memory T cells infiltration and survival in human lung cancer. J Immunother Cancer. 2020;8(2): e000778.
40. Reschke R, Gajewski TF. CXCL9 and CXCL10 bring the heat to tumors. Sci Immunol. 2022;7: eabq6509.
41. Prokhnevska N, Cardenas MA, Valanparambil RM, Sobierajska E, Barwick BG, Jansen C, Reyes Moon A, Gregorova P, delBalzo L, Greenwald R, et al. CD8(+) T cell activation in cancer comprises an initial activation phase in lymph nodes followed by effector differentiation within the tumor. Immunity. 2023;56:107-124.e105.
42. van Pul KM, Fransen MF, van de Ven R, de Gruijl TD. Immunotherapy goes local: the central role of lymph nodes in driving tumor infiltration and efficacy. Front Immunol. 2021;12: 643291.
43. Koukourakis MI, Giatromanolaki A. Tumor draining lymph nodes, immune response, and radiotherapy: towards a revisal of therapeutic principles. Biochim Biophys Acta Rev Cancer. 2022;1877: 188704.
44. Murphy TL, Murphy KM. Dendritic cells in cancer immunology. Cell Mol Immunol. 2022;19:3–13.
45. Meiser P, Knolle MA, Hirschberger A, de Almeida GP, Bayerl F, Lacher S, Pedde AM, Flommersfeld S, Hönninger J, Stark L, et al. A distinct stimulatory cDC1 subpopulation amplifies CD8(+) T cell responses in tumors for protective anti-cancer immunity. Cancer Cell. 2023;41:1498-1515.e1410.
46. Ferris ST, Ohara RA, Ou F, Wu R, Huang X, Kim S, Chen J, Liu TT, Schreiber RD, Murphy TL, Murphy KM. cDC1 vaccines drive tumor rejection by direct presentation independently of host cDC1. Cancer Immunol Res. 2022;10:920–31.

Publisher's Note